Mutant cycle analysis with modified saxitoxins reveals specific interactions critical to attaining high-affinity inhibition of hNa$_V$1.7

Rhiannon Thomas-Tran[a] and J. Du Bois[a,1]

[a]Department of Chemistry, Stanford University, Stanford, CA 94305

Edited by Richard W. Aldrich, The University of Texas at Austin, Austin, TX, and approved April 4, 2016 (received for review March 1, 2016)

Improper function of voltage-gated sodium channels (Na$_V$s), obligatory membrane proteins for bioelectrical signaling, has been linked to a number of human pathologies. Small-molecule agents that target Na$_V$s hold considerable promise for treatment of chronic disease. Absent a comprehensive understanding of channel structure, the challenge of designing selective agents to modulate the activity of Na$_V$ subtypes is formidable. We have endeavored to gain insight into the 3D architecture of the outer vestibule of Na$_V$ through a systematic structure–activity relationship (SAR) study involving the bis-guanidinium toxin saxitoxin (STX), modified saxitoxins, and protein mutagenesis. Mutant cycle analysis has led to the identification of an acetylated variant of STX with unprecedented, low-nanomolar affinity for human Na$_V$1.7 (hNa$_V$1.7), a channel subtype that has been implicated in pain perception. A revised toxin-receptor binding model is presented, which is consistent with the large body of SAR data that we have obtained. This new model is expected to facilitate subsequent efforts to design isoform-selective Na$_V$ inhibitors.

sodium channel | guanidinium toxin | mutant cycle analysis

Modulation of action potentials in electrically excitable cells is controlled by tight regulation of ion channel expression and distribution. Voltage-gated sodium ion channels (Na$_V$s) constitute one such family of essential membrane proteins, encoded in 10 unique genes (Na$_V$1.1–Na$_V$1.9, Na$_x$) and further processed through RNA splicing, editing, and posttranslational modification. Sodium channels are comprised of a large (~260 kDa) pore-forming α-subunit coexpressed with ancillary β-subunits. Misregulation and/or mutation of Na$_V$s have been ascribed to a number of human diseases including neuropathic pain, epilepsy, and cardiac arrhythmias. A desire to understand the role of individual Na$_V$ subtypes in normal and aberrant signaling motivates the development of small-molecule probes for regulating the function of specific channel isoforms (1–4).

Nature has provided a collection of small-molecule toxins, including (+)-saxitoxin (STX, **1**) and (−)-tetrodotoxin (TTX), which bind to a subset of mammalian Na$_V$ isoforms with nanomolar affinity (5–7). Guanidinium toxins inhibit Na^+ influx through Na$_V$s by occluding the outer pore above the ion selectivity filter (site 1). This proposed mechanism for toxin block follows from a large body of electrophysiological and site-directed mutagenesis studies (Fig. 1*A* and refs. 8–10). The detailed view of toxin binding, however, is unsupported by structural biology, as no high-resolution structure of a eukaryotic Na$_V$ has been solved to date (11–16). Na$_V$ homology models, constructed based on X-ray analyses of prokaryotic Na^+ and K^+ voltage-gated channels, do not sufficiently account for experimental structure–activity relationship (SAR) data (6, 17–20), and the molecular details underlying distinct differences in toxin potencies toward individual Na$_V$ subtypes remain undefined (5, 6, 21–23). The lack of structural information motivates a comprehensive, systematic study of toxin–protein interactions.

Double-mutant cycle analysis has proven an invaluable experimental method for assessing protein–protein, protein–peptide, and protein–small-molecule interactions in the absence of crystallographic data (Fig. 1*B* and Fig. S1 and refs. 9, 10, and 24–31). Herein, we describe mutant cycle analysis with Na$_V$s using STX and synthetically modified forms thereof. Our results are suggestive of a toxin–Na$_V$ binding pose distinct from previously published views. Our studies have resulted in the identification of a natural variant of STX that is potent against the STX-resistant human Na$_V$1.7 isoform (hNa$_V$1.7). Structural insights gained from these studies provide a foundation for engineering guanidinium toxins with Na$_V$ isoform selectivity.

Results

Methylated STX Analogs. Double-mutant cycle analysis of the STX binding site necessitates both ligand and protein modification. A collection of isomeric toxins bearing a methyl substituent group was targeted to ensure that relative differences in solvation energies between these compounds would be minimal. Variances in ligand affinity could thus be attributed to steric factors governing toxin–Na$_V$ interactions (32, 33). Previous bis-guanidinium toxin–Na$_V$ mutant cycle analyses have been limited to naturally occurring derivatives (9, 10). Accordingly, five monomethylated analogs (**2**–**5** and **8**, Table 1), along with two dimethylated variants (**6** and **9**) and decarbamoyl-STX (dcSTX, **7**) were prepared from L-serine methyl ester using routes adapted from our previously disclosed studies (34). Although naturally occurring STX derivatives with substitution at N7 or C13 appear in nature, to our knowledge no N9- or C10- natural product congeners have been identified (35–37).

Preliminary electrophysiological recordings to assess analog potencies were conducted with wild-type (WT) rat skeletal muscle α-subunit (rNa$_V$1.4) heterologously expressed in CHO

Significance

Chronic pain plagues at least 50 million Americans and has an estimated annual cost in excess of $200 billion. Consequently, there exists significant interest in developing effective, non-narcotic analgesics. Drugs that target individual voltage-gated sodium channel (Na$_V$) subtypes have appreciable therapeutic potential as pain medicines. Our work uses small-molecule design and protein mutagenesis to gain insight into the molecular architecture of the ion conduction pore of Na$_V$. These studies have revealed structural differences in the outer mouth of the channel that potentiate the binding of guanidinium toxins. Such findings are helping advance the preparation of isoform-selective Na$_V$ antagonists.

Author contributions: R.T.-T. and J.D.B. designed research; R.T.-T. performed research; R.T.-T. and J.D.B. analyzed data; and R.T.-T. and J.D.B. wrote the paper.

The authors declare no conflict of interest.

This article is a PNAS Direct Submission.

[1]To whom correspondence should be addressed. Email: jdubois@stanford.edu.

This article contains supporting information online at www.pnas.org/lookup/suppl/doi:10.1073/pnas.1603486113/-/DCSupplemental.

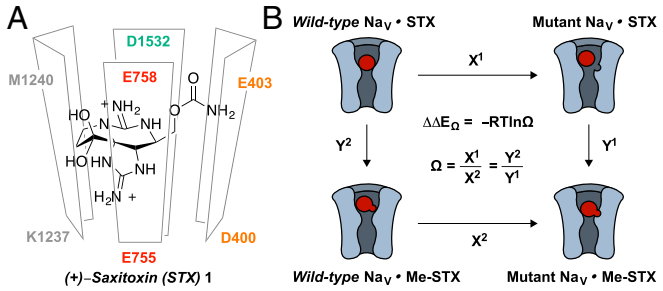

Fig. 1. (*A*) Schematic drawing of **1** bound in the Na$_V$ outer pore as suggested by previous electrophysiology and mutagenesis experiments. Each of the four domains (I, orange; II, red; III, gray; and IV, teal) is represented by a separate panel. (*B*) Schematic representation of double-mutant cycle analysis and mathematical definition of coupling energy ($\Delta\Delta E_\Omega$). X^1 = IC_{50}(WT·STX)/IC_{50}(MutNa$_V$·STX), X^2 = IC_{50}(WT·MeSTX)/IC_{50}(MutNa$_V$·MeSTX), Y^1 = IC_{50}(MutNa$_V$·STX)/IC_{50}(MutNa$_V$·MeSTX), and Y^2 = IC_{50}(WT·STX)/IC_{50}(WT·MeSTX).

cells (Table 1 and Fig. S2). Consistent with previous observations, N21 mono- and dimethylcarbamoylated derivatives **5** and **6** retain high affinity for rNa$_V$1.4, with IC_{50} values of 1.9 ± 0.1 nM and 4.5 ± 0.2 nM, respectively (38–41). In contrast, the introduction of a single methyl group on the tricyclic bis-guanidinium core of STX significantly reduces potency, between 74- and 300-fold for N7, N9, and C10 substitution (**2**–**4**). Concentration-response measurements for dcSTX **7** and C13-OAc STX **8** give intermediate IC_{50} values (35 ± 1.4 nM and 83 ± 3.9 nM, respectively), whereas the potency of isobutyrate **9** is substantially diminished (338 ± 9.3 nM). The 12-fold reduction in affinity of dcSTX **7** compared with STX is consistent with previous literature reports (7, 35). These data motivate further studies to interrogate the binding pose of guanidinium toxins in the outer vestibule of the conductance pore.

Mutant Cycle Analysis with Site 1 Mutants. To localize precise interactions responsible for high-affinity STX block of the channel, nine single-point Na$_V$1.4 mutants were initially prepared and characterized (Fig. 2, *SI Discussion*, and Fig. S1). Alanine residues were systematically introduced into the pore-loop region, above the Na^+ selectivity filter (i.e., DEKA loop), in all four domains (DI–DIV) of the channel. Given the large perturbations to STX binding previously reported when key carboxylate residues, E403 and E758, are neutralized, only aspartate mutations were introduced at these positions (8, 10). Single-point mutants generated measurable macroscopic currents (1–6 nA) and exhibited typical Na$_V$ gating kinetics when expressed in CHO cells. For each toxin–channel pair, concentration-response curves for I_{Na} block were obtained (Figs. S2 and S3). All amino acid mutations reduced the affinities of STX and methylated derivatives (**2**–**6** and **8**) compared with WT rNa$_V$1.4 (Table S1). Values of $\Delta\Delta E_\Omega$ obtained for methylated toxins are represented in Fig. 2. In select cases, IC_{50}s were estimated to be >50 μM and, consequently, $\Delta\Delta E_\Omega$ values were not determined.

No significant coupling interactions were measured between N7-Me STX **2** and N9-Me STX **3** and the pore-lining amino acids highlighted in Fig. 2 ($|\Delta\Delta E_\Omega| < 0.4$ kcal/mol). By contrast, the C10-Me compound **4** displayed $\Delta\Delta E_\Omega$ values of 1.7 ± 0.1 and 1.3 ± 0.1 kcal/mol with DI residues Y401 and E403, respectively. These interaction energies were the largest recorded among toxin derivatives **2**–**8** with any of the nine Ala mutants. Conversely, the relative affinities of N-methylcarbamate–modified toxins **5** and **6** against Na$_V$ mutants were similar to STX ($|\Delta\Delta E_\Omega| < 0.5$ kcal/mol).

Two toxin derivatives, dcSTX **7** and C13-OAc STX **8**, displayed notable coupling interactions with DIII residues. In experiments with the former compound, W1239A and Y401A afforded the largest $\Delta\Delta E_\Omega$ values ($\Delta\Delta E_\Omega$ of 0.9 ± 0.1 and 0.8 ± 0.1 kcal/mol, respectively), whereas ester **8** exhibited the most substantial coupling energies with W1239A and D1241A ($\Delta\Delta E_\Omega$ = 0.6 ± 0.1 and 0.6 ± 0.1 kcal/mol, respectively).

Additional Mutagenesis Reveals Localized Interactions Between C13-Modified Toxins and DIII. Amino acid substitution of DIII p-loop residues M1240 and D1241 has been found to significantly influence guanidinium toxin potency (6, 8). In previous work from our laboratory, STX resistance in primate Na$_V$1.7 was noted and ascribed to a natural variation of two pore-forming amino acids at positions 1240 and 1241. Given the modest coupling observed between C13-modified toxins **7** and **8** with DIII alanine mutants, as well as an interest in restoring bis-guanidinium toxin affinity to hNa$_V$1.7, nine additional single-point 1240 and 1241 Na$_V$1.4 mutants with amino acids of varying steric size and polarity were expressed (Fig. 3, Fig. S4, and Table S2). Position 1239 was left unperturbed, because substitution of this residue considerably destabilizes STX and STX derivative binding (all IC_{50}s >1.9 μM with W1239A).

Within the series of single-point M1240 mutants, threonine, serine, and isoleucine residues had the most demonstrable influence on dcSTX **7** and C13-OAc STX **8** affinity (Fig. 3*A*). For the former two amino acids, the magnitude of $\Delta\Delta E_\Omega$ was markedly greater for acetylated toxin **8** than for decarbamoylated toxin **7** (M1240T, $\Delta\Delta E_\Omega$ = 2.7 ± 0.1 kcal/mol versus 0.9 ± 0.1 kcal/mol; M1240S, $\Delta\Delta E_\Omega$ = 1.4 ± 0.1 kcal/mol versus 0.6 ± 0.1 kcal/mol). Mutation of M1240 to an H-bond donor did not adversely influence the affinity of derivatives **7** and **8** to the same extent as STX, which displayed 29- and 63-fold reduced potency against Thr and Ser mutants, respectively (Fig. S4 and Table S2). For all other M1240 mutants, binding of compound **7** was destabilized relative to STX, as revealed by negative interaction energies ($\Delta\Delta E_\Omega$ = −0.8 to −0.2 kcal/mol; Table S2). Conversely, mutant cycle analysis with acetate ester derivative **8** gave coupling values ranging from −0.1 to 1.0 kcal/mol for all other M1240 single-point mutants. The increasing magnitude of $\Delta\Delta E_\Omega$ for analog **8** follows the trend Asn < Ala < Val < Ile < Ser < Thr.

At position 1241, the most favorable DIII interactions were recorded for isoleucine, threonine, and asparagine mutants with compound **8** ($\Delta\Delta E_\Omega$ of 1.5 ± 0.1, 1.0 ± 0.1, and 0.9 ± 0.1 kcal/mol, respectively; Fig. 3*A*). Replacement of D1241 with a neutral

Table 1. Affinities of STX and analogs 2–8 for rNa$_V$1.4 determined by whole-cell voltage-clamp electrophysiology

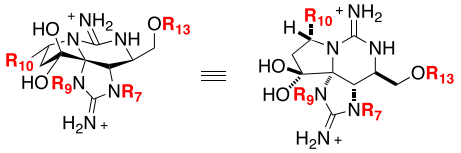

Compound	R^7	R^9	R^{10}	R^{13}	WT rNa$_V$1.4 IC_{50}, nM
1	H	H	H	C(O)NH$_2$	2.9 ± 0.1
2	Me	H	H	C(O)NH$_2$	370 ± 50
3	H	Me	H	C(O)NH$_2$	879 ± 53
4	H	H	Me	C(O)NH$_2$	215 ± 16
5	H	H	H	C(O)NHMe	1.9 ± 0.1
6	H	H	H	C(O)NMe$_2$	4.5 ± 0.2
7	H	H	H	H	35 ± 1.4
8	H	H	H	C(O)Me	83 ± 3.9
9	H	H	H	C(O)CHMe$_2$	338 ± 9.3

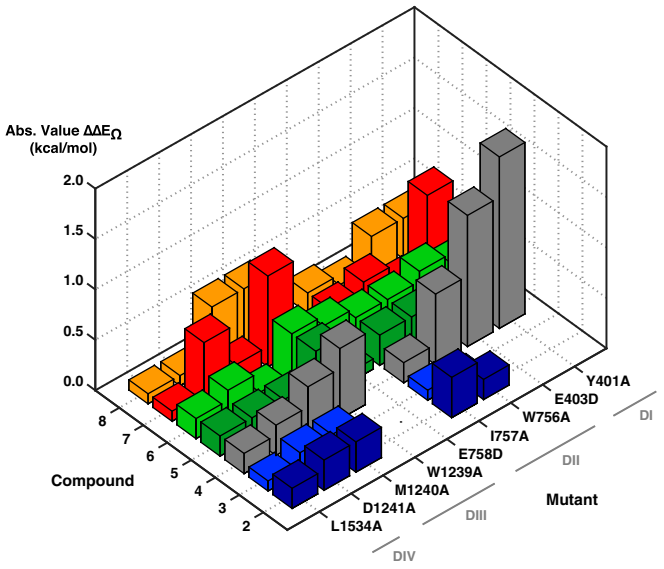

Fig. 2. Mutant cycle analysis with compounds **2**–**8** and Na_V single-point mutants. $\Delta\Delta E_\Omega$ absolute values are shown in units of kilocalories per mole. Dose–response curves, relative inhibition constants (IC_{50}s), and SEM for calculations are given in Fig. S2 and Table S1.

residue (Ala and Ile) resulted in an eight- and 22-fold decrease in STX IC_{50} values, compared with a ninefold and 1.5-fold reduction in the affinity of ester **8**. With the exception of the D1241I mutant, the relative potency of dcSTX **7** was not strongly influenced by 1241 substitution ($\Delta\Delta E_\Omega < 0.6$ kcal/mol).

C13-Modified Toxins Are Potent Against 1240/1241 Double Mutants. Because both C13 derivatives **7** and **8** displayed $\Delta\Delta E_\Omega$ values ≥1.0 kcal with $Na_V1.4$ M1240T and D1241I, additional binding studies were performed using the corresponding double-point mutant channel (Fig. 3*B*, Fig. S4, and Table S2). This construct is structurally analogous to the outer vestibule of primate $Na_V1.7$, which expresses Thr and Ile in DIII of the p-loop (6). Coupling energies for STX analogs **7** and **8**, in addition to isobutyrate ester **9**, against $Na_V1.4$ M1240T/D1241I are quite large, with values of 2.1 ± 0.1 kcal/mol, 4.2 ± 0.1 kcal/mol, and 2.0 ± 0.1, respectively (Tables S2 and S3). Notably, the affinity of C13-OAc STX **8** for this mutant Na_V is threefold greater than for the WT channel (IC_{50} = 26 ± 2.3 nM versus 83 ± 3.9 nM). Similar results, albeit with diminished absolute magnitudes for $\Delta\Delta E_\Omega$, were obtained from mutant cycle analysis with N21-dimethyl STX **6** (Fig. 3*B*, Fig. S4, and Table S2). Data gathered from experiments with two additional $Na_V1.4$ double mutants, M1240A/D1241A and M1240T/D1241A, and compounds **6**–**9** followed analogous trends (Fig. S4 and Tables S2 and S3).

To further define toxin–DIII interactions, additional mutant cycles with isobutyrate ester **9** were analyzed (Table S3). Binding energies for toxin derivatives **6** and **8** with $rNa_V1.4$ were used as starting values for these cycles to directly probe steric constraints within DIII. Coupling of the branched ester **9** to M1240T/D1241I was modest compared with dimethylcarbamate **6** ($\Delta\Delta E_\Omega$ = 0.7 ± 0.1 kcal/mol) but significantly diminished ($\Delta\Delta E_\Omega = -2.2 \pm 0.1$ kcal/mol) relative to C13-acetate derivative **8**.

Previously reported docking models for STX have positioned C10 and C11 proximal to the pore loop of DIII (6, 17–20). Accordingly, C10-Me STX **4** was tested against $Na_V1.4$ M1240T/D1241I in addition to other DIII mutant constructs (Fig. 3*B*, Fig. S4, and Table S2). The largest $\Delta\Delta E_\Omega$ of 0.8 kcal/mol was obtained for **4** against the 1240T/1241I double mutant, a value that is decidedly smaller than coupling energies calculated for **6**, **7**, and **8** (Fig. 3*B*).

C13-OAc STX 8 Retains High Affinity for $hNa_V1.7$. Given the potency of C13-OAc STX **8** for the $Na_V1.4$ M1240T/D1241I double mutant (IC_{50} = 26 ± 2.3 nM), this compound was tested against human nociceptive $Na_V1.7$ ($hNa_V1.7$) stably expressed in HEK cells. An IC_{50} of 19 ± 1.7 nM (Fig. 3 *C* and *D* and Fig. S5) was measured, a value similar to that obtained from experiments

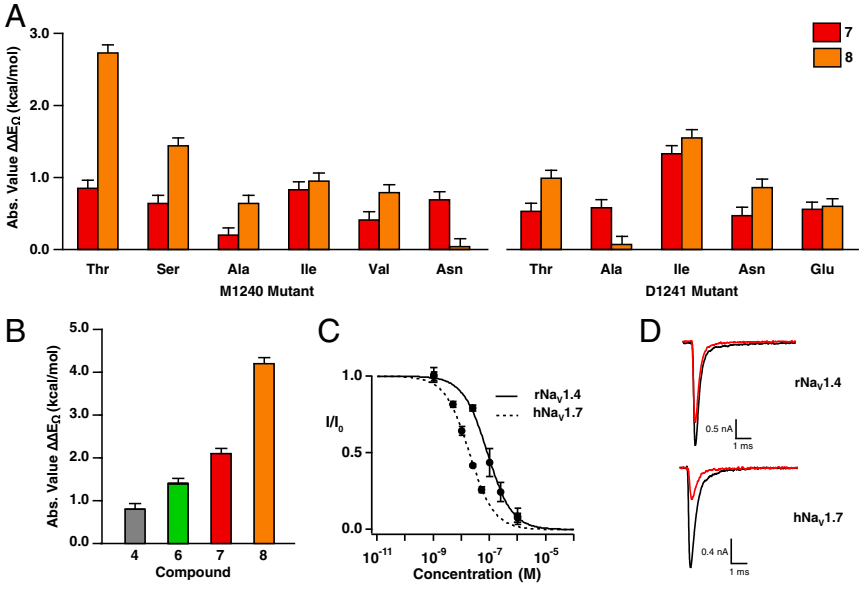

Fig. 3. Additional mutagenesis of M1240 and D1241 reveals interactions responsible for coupling of C13-substituents to DIII. (*A*) Absolute values of $\Delta\Delta E_\Omega$ (kilocalories per mole) for compounds **7** and **8** with M1240 and D1241 single-point mutants. (*B*) Absolute values of $\Delta\Delta E_\Omega$ (kilocalories per mole) for compounds **4**, **6**, **7**, and **8** with the $rNa_V1.4$ M1240T/D1241I double-point mutant. (*C*) Concentration response curves for current inhibition of $rNa_V1.4$ (solid line) and $hNa_V1.7$ (dotted line) by **8** determined by whole-cell voltage-clamp electrophysiology. (*D*) Current recordings elicited by a 10-ms voltage step from −100 to 0 mV before (black) and following (red) application of 25 nM **8** to CHO cells expressing $rNa_V1.4$ (*Top*) and HEK cells expressing $hNa_V1.7$ (*Bottom*). WT $rNa_V1.4$ and STX were used as references in $\Delta\Delta E_\Omega$ calculations.

with $Na_V1.4$ M1240T/D1241I. By comparison with binding data recorded with other WT isoforms ($rNa_V1.2$, $rNa_V1.4$, and $hNa_V1.5$), C13-OAc STX **8** is two- to 240-fold more selective for the 1.7 channel (Fig. S5).

Discussion

Small molecules that functionally "knock out" specific Na_V isoforms hold promise as tools for exploring the role of individual channel subtypes in modulating compound action potentials. The development of such inhibitors through rational design, however, is challenged by the absence of crystallographic data for eukaryotic Na_Vs. To obtain structural insights into the molecular determinants that govern high-affinity Na_V block by bis-guanidinium toxins, mutant cycle analysis was performed with six, nonnatural methylated saxitoxin derivatives, as well as dcSTX and C13-OAc STX, 18 single-point and 3 double-point $Na_V1.4$ mutants. Significant coupling energies (>1 kcal/mol) were calculated for multiple toxin–mutant channel pairs (Figs. 2 and 3). These data have led to us to propose a new toxin–receptor docking model.

An initial screen of p-loop mutants (Fig. 2) with modified STX analogs showed evident coupling interactions between residues in DI (Y401A and E403D) and the C10-Me derivative **4**. Additionally, compounds altered at C13, dcSTX **7** and C13-OAc STX **8**, displayed modest coupling with alanine mutants of DIII residues W1239, M1240, and D1241. These results, together with a previous report by our laboratory detailing STX–$hNa_V1.7$ binding and the importance of DIII residues in defining guanidinium toxin affinity (6), prompted further study of compounds **7** and **8** against a number of M1240 and D1241 single-point mutants (Fig. 3*A*). In these experiments, significant interaction energies (≥1.4 kcal/mol) were computed for C13-OAc STX **8** with M1240T and M1240S and for both dcSTX **7** and C13-OAcSTX **8** with D1241I (≥1.3 kcal/mol).

Differences in the polarity and steric size of C13-modified toxins **7** and **8** compared with STX, as well as within DIII mutant channels, provide rationale for the relative potencies of the three ligands. Low-nanomolar block of Na_Vs by STX requires a large, hydrophobic amino acid residue at position 1240 and an acidic residue at position 1241. Replacing M1240 with smaller, polar groups such as Thr and Ser substantially perturbs STX binding, decreasing respective IC_{50} values by 29-fold and 63-fold. Conversely, C13-OAc STX **8** binds with threefold increased potency to the M1240T mutant channel. In the case of position 1241, neutralization of the Asp residue to Ile, Asn, or Glu has a more profound influence on STX binding than on the acetate ester analog.

The striking results with dcSTX **7** and C13-OAc STX **8** and DIII single-point mutants compelled us to perform subsequent investigations of M1240/D1241 double-point mutant channels (Fig. 3*B*). Ester **8** binds to $rNa_V1.4$ M1240T/D1241I with high affinity, exhibiting threefold greater potency toward this double mutant than WT $rNa_V1.4$. Compared with STX, acetate **8** is 44 times more potent against this same mutant channel. These observed differences in affinity are recapitulated against native $hNa_V1.7$ (Fig. 3 *C* and *D*), which contains threonine and isoleucine at structurally equivalent positions to 1240 and 1241 in $rNa_V1.4$. To the best of our knowledge, compound **8** represents the first example of an STX variant with low-nanomolar potency against $hNa_V1.7$.

Previous homology models of the Na_V pore with STX bound have posited three key electrostatic interactions between (*i*) the five-membered ring guanidinium and E755, (*ii*) the six-membered ring guanidinium and D1532, and (*iii*) the C12-hydrated ketone and E758 (6, 17–20). These contacts, defined by experimental comparison of STX and TTX affinity for site 1 mutants, enforce close packing between positions C10 and C11 on STX and DIII p-loop residues (Figs. 1*A* and 4*A*). Mutant cycle analysis with C10- and C13-modified toxins, however, suggests an alternative pose in which C10 is proximal to DI and C13 is in contact with DIII (Fig. 4 *B* and *C*). In this docking model, the five-membered ring guanidinium group is proximal to E755; the hydrated ketone at C12 is proposed to hydrogen bond with D1532 and the six-membered ring guanidinium forms a salt bridge with E758. Thus, all three principal contacts between toxin and receptor are maintained.

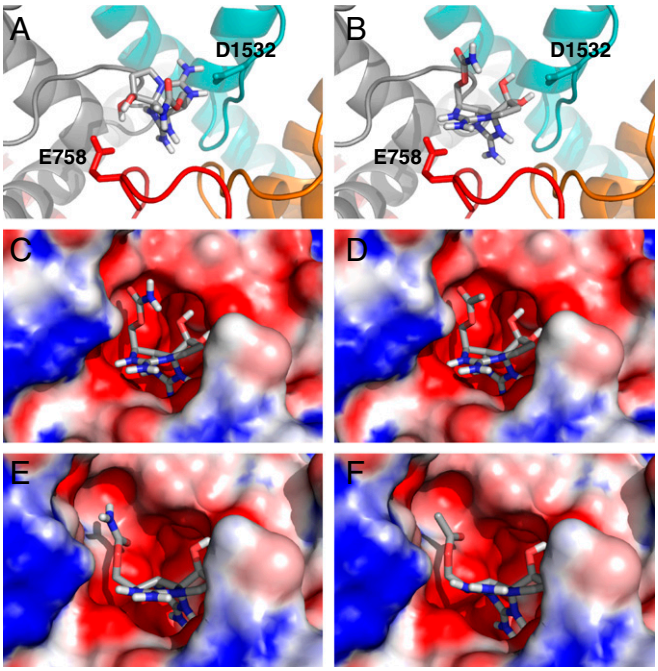

Fig. 4. Docking of STX at site 1 of $rNa_V1.4$ in the canonical (*A*) and proposed (*B*) orientations. The four domains are shown in cartoon representations and colored orange (DI), red (DII), gray (DIII), and teal (DIV). Images highlighting the differences between electrostatic potential surfaces of STX (*C*) and C13-OAc STX **8** (*D*) docked to the $rNa_V1.4$ outer pore in the proposed orientation. Equivalent images showing STX (*E*) and C13-OAc STX **8** (*F*) in the binding pocket of the M1240T/D1241I double mutant. Depicted potential range is −20 (red) to +5 kT (blue). Toxin structures generated using OMEGA version 2.5.1; docking performed with OEDocking version 3.0.1 (OpenEye Scientific Software, www.eyesopen.com).

Shape complementarity and hydrogen bonding between the C13-carbamate in STX and DIII D1241 favor close positioning of these groups. In this same orientation, binding of C13-OAc STX **8** to WT $Na_V1.4$ is destabilized relative to STX owing to the less polar nature of the ester group (Fig. 4*D* and Dataset S1). Conversely, in the M1240T/D1241I mutant channel, the strength of the C13-carbamate interaction with DIII residues is mitigated (Fig. 4*E*). The ester derivative **8** displays higher affinity for this double mutant (threefold relative to $rNa_V1.4$), presumably due to the increased hydrophobicity of the binding pocket and the presence of a hydrogen bond donor in Thr (Fig. 4*F* and Dataset S2). In this model, differences in binding affinity between the acetate **8** and isobutyrate **9** may be ascribed to the small volume cleft between DIII and DIV, which does not easily accommodate the sterically large, branched isopropyl group. On the other hand, the perturbation to binding caused by the planar N21-dimethylated carbamate (i.e., **6**) is minimal.

More than one explanation may account for differences between our revised STX docking model and those previously published. In prior work, specific constraints imposed on bis-guanidinium contacts with carboxylate residues E755, E758, and D1532 limited the sampling of STX poses (6, 17–20). By relaxing these constraints, we have identified an alternative ligand binding model that accounts for our SAR data as well as previous results of this type (9, 10). It is possible, however, that STX and

STX analogs adopt more than one high-affinity binding arrangement within the mouth of the channel. In native $rNa_V1.4$, the canonical STX binding model may indeed be preferred, but in certain mutant Na_Vs or with specific STX derivatives the docking orientation suggested by our findings could be favored (42–44). The potential of bis-guanidinium toxins to occlude site 1 through disparate binding modes presents an unusual challenge for engineering subtype-selective inhibitors of Na_V function around this chemotype.

Access to STX derivatives through chemical synthesis has facilitated a systematic investigation of toxin–receptor interactions that govern potent Na_V block. Mutant cycle analysis has revealed unexpected nearest-neighbor contacts between modified toxins and DI and DIII p-loop amino acids that are not explained by existing models of STX lodged in the channel pore. These data have led us to propose an alternative bis-guanidinium toxin binding model, which could aid future efforts to design subtype-specific ligands. Our studies have also resulted in the identification of C13-OAc STX, a naturally occurring derivative of STX that displays selective, high-affinity block of both the $rNa_V1.4$ M1240T/D1241I mutant channel and the human $Na_V1.7$ isoform. To our knowledge, these findings provide the first proof of concept for engineering Na_V-subtype-specific inhibitors around the site 1 locus.

Materials and Methods

Toxin Synthesis. Toxins were prepared from L-serine methyl ester according to a previously reported route (34). All reagents used were obtained commercially unless otherwise noted. Final compounds were purified using semipreparative HPLC performed on a Varian ProStar model 210. Characterization information for modified toxins can be found in *SI Materials and Methods*.

Cell Culture and Electrophysiology. Electrophysiology experiments were conducted using CHO cells transiently expressing the α-subunit of rat $Na_V1.4$ ($rNa_V1.4$) or mutant thereof (45), human $Na_V1.5$ ($hNa_V1.5$), rat $Na_V1.2$ ($rNa_V1.2$), or HEK cells stably expressing the α-subunit of human $Na_V1.7$ ($hNa_V1.7$). Cell culture was performed as described previously (38). Additional information can be found in *SI Materials and Methods*.

Sodium currents were measured using the patch-clamp technique in the whole-cell configuration with an Axopatch- 200b amplifier (Axon Instruments), as previously described by Moran et al. (46). Borosilicate glass micropipettes (Sutter Instruments) were fire-polished to a tip diameter yielding a resistance of 1.2–3.0 MΩ in the working solutions. For CHO cells, the micropipette was filled with 40 mM NaF, 1 mM EDTA, 20 mM Hepes, and 125 mM CsCl. The external solution had the following composition: 160 mM NaCl, 2 mM $CaCl_2$, and 20 mM Hepes. For HEK cells, the micropipette was filled with 10 mM NaF, 10 mM NaCl, 1.1 mM EGTA, 10 mM Hepes, and 130 mM CsF. The external solution had the following composition: 140 mM NaCl, 3 mM KCl, 1 mM $CaCl_2$, 1 mM $MgCl_2$, and 10 mM Hepes. The pH of all solutions was adjusted to 7.4 with 50 wt % aqueous CsOH.

The output of the patch-clamp amplifier was filtered with a built-in low-pass, four-pole Bessel filter having a cutoff frequency of 10 kHz and sampled at 100 kHz. The membrane was kept at a holding potential of –100 mV. Pulse stimulation and data acquisition used 16 bit D–A and A–D converters (Digidata 1322A; Axon Instruments) controlled with the PClamp software (Axon Instruments). Leak currents were subtracted using a standard P/4 protocol of the same polarity. Access resistance was always <4 MΩ and the cell capacitance was between 4 and 20 pF, as measured by the compensating circuit of the amplifier. The series resistance was typically compensated between 80% and 85%. All measurements were done at room temperature (20–22 °C). Recordings were made at least 5 min after establishing the whole-cell and voltage-clamp configuration to allow for stabilization of the voltage-dependent properties of the channels. Currents were elicited by 10-ms step depolarizations from a holding potential of –100 mV to 0 mV. Data were normalized to control currents, plotted against toxin concentration, and analyzed using custom software developed in the Igor environment (Wavemetrics). Data were fit to Langmuir isotherms to elicit IC_{50} values and expressed as mean ± SD. The number of observations (n) was ≥3 for all reported data and statistical comparisons were performed using two-tailed Student's t tests assuming unequal variances.

Mutagenesis. Primers were synthesized by the Protein and Nucleic Acid Facility at Stanford University. Primer sequences can be found in *SI Materials and Methods*. Mutants M1240T, D1241I, and M1240T/D1241I were prepared as previously reported (6). Site-directed mutagenesis was performed using either the QuikChange II XL or QuikChange Lightening kit (Agilent Technologies) according to the manufacturer's protocols. Double and triple mutants were prepared by iterative single mutations. Mutations were confirmed by DNA sequencing (Sequetech) of the appropriate section of the resulting plasmid.

Mutant Cycle Analysis. Interaction energies ($\Delta\Delta E_\Omega$s) were calculated according to Hidalgo and MacKinnon (*SI Discussion*, Fig. S1, and ref. 25). SEs for $\Delta\Delta E_\Omega$ were calculated from the experimental error of the measured IC_{50} values using the geometric sum of the partial errors (9). A positive $\Delta\Delta E_\Omega$ indicates that the mutated pair (i.e., modified toxin and channel mutant) has a greater binding energy relative to the native pair (i.e., STX and WT $rNa_V1.4$), the result of either addition of a stabilizing interaction or removal of a repulsive interaction upon mutation.

Ligand Docking. Docking experiments were performed using homology models of the pore structure for WT $rNa_V1.4$ and M1240T/D1241I double-point mutants previously reported by Walker et al. (6). Computational ligand preparation was accomplished using OMEGA version 2.5.1 and docking was performed with the FRED prediction tool in the OEDocking (version 3.0.1) suite (OpenEye Scientific Software) (47, 48).

ACKNOWLEDGMENTS. We thank M. Maduke for generous use of laboratory space and equipment and W. H. Parsons for helpful discussions. This work was supported by National Institutes of Health Grant R01-NS045684 and by Pfizer. R.T-T. is a National Science Foundation Predoctoral Fellow.

1. Akopian AN, et al. (1999) The tetrodotoxin-resistant sodium channel SNS has a specialized function in pain pathways. *Nat Neurosci* 2(6):541–548.
2. Planells-Cases R, et al. (2000) Neuronal death and perinatal lethality in voltage-gated sodium channel alpha(II)-deficient mice. *Biophys J* 78(6):2878–2891.
3. Nassar MA, et al. (2004) Nociceptor-specific gene deletion reveals a major role for $Na_v1.7$ (PN1) in acute and inflammatory pain. *Proc Natl Acad Sci USA* 101(34): 12706–12711.
4. Eijkelkamp N, et al. (2012) Neurological perspectives on voltage-gated sodium channels. *Brain* 135(Pt 9):2585–2612.
5. Thottumkara AP, Parsons WH, Du Bois J (2014) Saxitoxin. *Angew Chem Int Ed Engl* 53(23):5760–5784.
6. Walker JR, et al. (2012) Marked difference in saxitoxin and tetrodotoxin affinity for the human nociceptive voltage-gated sodium channel ($Na_v1.7$) [corrected]. *Proc Natl Acad Sci USA* 109(44):18102–18107.
7. Alonso E, Alfonso A, Vieytes MR, Botana LM (2016) Evaluation of toxicity equivalent factors of paralytic shellfish poisoning toxins in seven human sodium channels types by an automated high throughput electrophysiology system. *Arch Toxicol* 90(2):479–488.
8. Penzotti JL, Fozzard HA, Lipkind GM, Dudley SC, Jr (1998) Differences in saxitoxin and tetrodotoxin binding revealed by mutagenesis of the Na^+ channel outer vestibule. *Biophys J* 75(6):2647–2657.
9. Penzotti JL, Lipkind G, Fozzard HA, Dudley SC, Jr (2001) Specific neosaxitoxin interactions with the Na^+ channel outer vestibule determined by mutant cycle analysis. *Biophys J* 80(2):698–706.
10. Choudhary G, Shang L, Li X, Dudley SC, Jr (2002) Energetic localization of saxitoxin in its channel binding site. *Biophys J* 83(2):912–919.
11. Sato C, et al. (2001) The voltage-sensitive sodium channel is a bell-shaped molecule with several cavities. *Nature* 409(6823):1047–1051.
12. Payandeh J, Scheuer T, Zheng N, Catterall WA (2011) The crystal structure of a voltage-gated sodium channel. *Nature* 475(7356):353–358.
13. Zhang X, et al. (2012) Crystal structure of an orthologue of the NaChBac voltage-gated sodium channel. *Nature* 486(7401):130–134.
14. Payandeh J, Gamal El-Din TM, Scheuer T, Zheng N, Catterall WA (2012) Crystal structure of a voltage-gated sodium channel in two potentially inactivated states. *Nature* 486(7401):135–139.
15. McCusker EC, et al. (2012) Structure of a bacterial voltage-gated sodium channel pore reveals mechanisms of opening and closing. *Nat Commun* 3:1102.
16. Ahuja S, et al. (2015) Structural basis of $Na_v1.7$ inhibition by an isoform-selective small-molecule antagonist. *Science* 350(6267):aac5464.
17. Lipkind GM, Fozzard HA (2000) KcsA crystal structure as framework for a molecular model of the Na^+ channel pore. *Biochemistry* 39(28):8161–8170.
18. Tikhonov DB, Zhorov BS (2005) Modeling P-loops domain of sodium channel: Homology with potassium channels and interaction with ligands. *Biophys J* 88(1):184–197.
19. Scheib H, et al. (2006) Modeling the pore structure of voltage-gated sodium channels in closed, open, and fast-inactivated conformation reveals details of site 1 toxin and local anesthetic binding. *J Mol Model* 12(6):813–822.

20. Tikhonov DB, Zhorov BS (2012) Architecture and pore block of eukaryotic voltage-gated sodium channels in view of NavAb bacterial sodium channel structure. *Mol Pharmacol* 82(1):97–104.
21. Heinemann SH, Terlau H, Imoto K (1992) Molecular basis for pharmacological differences between brain and cardiac sodium channels. *Pflugers Arch* 422(1):90–92.
22. Rosker C, et al. (2007) The TTX metabolite 4,9-anhydro-TTX is a highly specific blocker of the $Na_v1.6$ voltage-dependent sodium channel. *Am J Physiol Cell Physiol* 293(2): C783–C789.
23. Santarelli VP, Eastwood AL, Dougherty DA, Horn R, Ahern CA (2007) A cation-π interaction discriminates among sodium channels that are either sensitive or resistant to tetrodotoxin block. *J Biol Chem* 282(11):8044–8051.
24. Schreiber G, Fersht AR (1995) Energetics of protein-protein interactions: Analysis of the barnase-barstar interface by single mutations and double mutant cycles. *J Mol Biol* 248(2):478–486.
25. Hidalgo P, MacKinnon R (1995) Revealing the architecture of a K^+ channel pore through mutant cycles with a peptide inhibitor. *Science* 268(5208):307–310.
26. Hong L, Kim IH, Tombola F (2014) Molecular determinants of Hv1 proton channel inhibition by guanidine derivatives. *Proc Natl Acad Sci USA* 111(27):9971–9976.
27. Desaphy J-F, et al. (2012) Molecular insights into the local anesthetic receptor within voltage-gated sodium channels using hydroxylated analogs of mexiletine. *Front Pharmacol* 3:17.
28. Dudley SC, Jr, et al. (2000) μ-conotoxin GIIIA interactions with the voltage-gated Na^+ channel predict a clockwise arrangement of the domains. *J Gen Physiol* 116(5):679–690.
29. Chang NS, French RJ, Lipkind GM, Fozzard HA, Dudley S, Jr (1998) Predominant interactions between μ-conotoxin Arg-13 and the skeletal muscle Na^+ channel localized by mutant cycle analysis. *Biochemistry* 37(13):4407–4419.
30. Cohen L, et al. (2007) Design of a specific activator for skeletal muscle sodium channels uncovers channel architecture. *J Biol Chem* 282(40):29424–29430.
31. Yang F, et al. (2015) Structural mechanism underlying capsaicin binding and activation of the TRPV1 ion channel. *Nat Chem Biol* 11(7):518–524.
32. Pirrung MC, et al. (2005) Methyl scanning: Total synthesis of demethylasterriquinone B1 and derivatives for identification of sites of interaction with and isolation of its receptor(s). *J Am Chem Soc* 127(13):4609–4624.
33. Chatterjee J, Gilon C, Hoffman A, Kessler H (2008) N-methylation of peptides: A new perspective in medicinal chemistry. *Acc Chem Res* 41(10):1331–1342.
34. Mulcahy JV, Du Bois J (2008) A stereoselective synthesis of (+)-gonyautoxin 3. *J Am Chem Soc* 130(38):12630–12631.
35. Onodera H, Satake M, Oshima Y, Yasumoto T, Carmichael WW (1997) New saxitoxin analogues from the freshwater filamentous cyanobacterium *Lyngbya wollei*. *Nat Toxins* 5(4):146–151.
36. Yotsu-Yamashita M, et al. (2004) The structure of zetekitoxin AB, a saxitoxin analog from the Panamanian golden frog Atelopus zeteki: A potent sodium-channel blocker. *Proc Natl Acad Sci USA* 101(13):4346–4351.
37. Wiese M, D'Agostino PM, Mihali TK, Moffitt MC, Neilan BA (2010) Neurotoxic alkaloids: Saxitoxin and its analogs. *Mar Drugs* 8(7):2185–2211.
38. Andresen BM, Du Bois J (2009) De novo synthesis of modified saxitoxins for sodium ion channel study. *J Am Chem Soc* 131(35):12524–12525.
39. Ondrus AE, et al. (2012) Fluorescent saxitoxins for live cell imaging of single voltage-gated sodium ion channels beyond the optical diffraction limit. *Chem Biol* 19(7): 902–912.
40. Parsons WH, Du Bois J (2013) Maleimide conjugates of saxitoxin as covalent inhibitors of voltage-gated sodium channels. *J Am Chem Soc* 135(29):10582–10585.
41. Hoehne A, et al. (2013) A ^{18}F-labeled saxitoxin derivative for in vivo PET-MR imaging of voltage-gated sodium channel expression following nerve injury. *J Am Chem Soc* 135(48):18012–18015.
42. Mewshaw RE, et al. (2005) ERbeta ligands. 3. Exploiting two binding orientations of the 2-phenylnaphthalene scaffold to achieve ERbeta selectivity. *J Med Chem* 48(12): 3953–3979.
43. Pei Z, et al. (2006) Discovery, structure-activity relationship, and pharmacological evaluation of (5-substituted-pyrrolidinyl-2-carbonyl)-2-cyanopyrrolidines as potent dipeptidyl peptidase IV inhibitors. *J Med Chem* 49(12):3520–3535.
44. Mobley DL, Dill KA (2009) Binding of small-molecule ligands to proteins: "What you see" is not always "what you get". *Structure* 17(4):489–498.
45. Bennett E, Urcan MS, Tinkle SS, Koszowski AG, Levinson SR (1997) Contribution of sialic acid to the voltage dependence of sodium channel gating. A possible electrostatic mechanism. *J Gen Physiol* 109(3):327–343.
46. Moran O, Picollo A, Conti F (2003) Tonic and phasic guanidinium toxin-block of skeletal muscle Na channels expressed in mammalian cells. *Biophys J* 84(5): 2999–3006.
47. Hawkins PCD, Skillman AG, Warren GL, Ellingson BA, Stahl MT (2010) Conformer generation with OMEGA: Algorithm and validation using high quality structures from the Protein Databank and Cambridge Structural Database. *J Chem Inf Model* 50(4): 572–584.
48. Hawkins PCD, Nicholls A (2012) Conformer generation with OMEGA: Learning from the data set and the analysis of failures. *J Chem Inf Model* 52(11):2919–2936.